Er^{3+} doped phosphoniobate glasses and planar waveguides: structural and optical properties

2008 J. Phys.: Condens. Matter 20 285224

(http://iopscience.iop.org/0953-8984/20/28/285224)

J. Phys.: Condens. Matter **20** (2008) 285224 (8pp) doi:10.1088/0953-8984/20/28/285224

Er^{3+} doped phosphoniobate glasses and planar waveguides: structural and optical properties

A J Barbosa[1], F A Dias Filho[1], L J Q Maia[1], Y Messaddeq[1], S J L Ribeiro[1,3] and R R Gonçalves[2]

[1] Institute of Chemistry, São Paulo State University—UNESP-CP 355, Araraquara-SP, 14801-970, Brazil

[2] Department of Chemistry, FFCLRP, University of São Paulo—USP, Ribeirão Preto-SP, 14040-901, Brazil

E-mail: sidney@iq.unesp.br (S J L Ribeiro)

Received 8 March 2008, in final form 4 June 2008
Published 24 June 2008
Online at stacks.iop.org/JPhysCM/20/285224

Abstract

Phosphoniobate glasses with composition (mol%) $(100 - x)NaPO_3$–xNb_2O_5 (x varying from 11 to 33) were prepared and characterized by means of thermal analysis, Fourier transform infrared spectroscopy, Raman scattering and ^{31}P nuclear magnetic resonance. The addition of Nb_2O_5 to the polyphosphate base glass leads to depolymerization of the metaphosphate structure. Different colors were observed and assigned as indicating the presence of Nb^{4+} ions, as confirmed by electron paramagnetic resonance measurements. The color was observed to depend on the glass composition and melting temperature as well. Er^{3+} containing samples were also prepared. Strong emission in the 1550 nm region was observed. The Er^{3+} $^4I_{15/2}$ emission quantum efficiency was observed to be 90% and the quenching concentration was observed to be 1.1 mol% (1.45×10^{20} ions cm^{-3}). Planar waveguides were prepared by Na^+–K^+–Ag^+ ion exchange with Er^{3+} containing samples. Optical parameters of the waveguides were measured at 632.8, 543.5 and 1550 nm by the prism coupling technique as a function of the ion exchange time and Ag^+ concentration. The optimized planar waveguides show a diffusion depth of 5.9 μm and one propagating mode at 1550 nm.

(Some figures in this article are in colour only in the electronic version)

1. Introduction

Glasses are promising materials for photonic applications. In particular, erbium doped glasses have been used to produce optical fiber amplifiers operating successfully in the C telecommunication band [1, 2]. Growing activity in this field is followed by a significant increase in development of new planar waveguide systems including passive and active optical components, based on rare-earth doped glasses for all optical applications [3, 4]. In this way, research into innovative materials has received attention—comprising the processes for development of compact and integrated optical devices as well as techniques of characterization—in order to obtain a final material with optimized physical and chemical properties.

[3] Author to whom any correspondence should be addressed.

Phosphate glasses have received attention because of their unique properties. They have higher transmission in the ultraviolet region compared to silicate glasses [5] and have been investigated as rare-earth ion host matrices in laser systems [6], optical fibers and lenses [7, 8] and planar waveguides [9]. The poor chemical durability of these early optical glasses limited their applications and has discouraged their further development [5]. However, the introduction of niobium oxide in phosphate glasses has led to increasing mechanical and chemical stability. Er^{3+}–Yb^{3+} doped phosphoniobate glasses have been studied where infrared emission together with visible up-conversion has been considered [10].

As regards planar waveguides, among several physical and chemical deposition techniques like flame hydrolysis,

Table 1. Sample identification and compositions ($x$$Nb_2O_5$-$(1-x)$$NaPO_3$ glasses (mol%)), glass transition temperature, T_g (°C), density (g cm^{-1}), optical band gap (eV) and cut-off wavelength (nm).

Sample (x)	T_g (±0.5 °C)	Density (g cm^{-3})	Band gap (±0.01 eV)	Cut-off (nm)
N11(11.1)	470.8	2.7984	3.78	328
N14(14.3)	506.2	2.8821	3.76	330
N17(17.7)	581.2	2.9712	3.73	333
N21(21.2)	631.2	3.0641	3.67	338
N25(25.0)	675.0	3.1575	3.61	344
N29(29.0)	700.0	3.1575	3.51	354
N33(33.3)	708.3	—	3.41	354

chemical vapor deposition, glass sputtering, sol–gel and ion implantation, the ion exchange represents one of the most commonly used [11–14]. The preparation of planar waveguides by ion exchange requires chemically stable, high optical quality glasses containing sufficiently high alkali metal ion concentration [14]. Additionally, in active planar waveguides for miniature devices the rare-earth solubility becomes an important factor, where a short optical path requires large active Er^{3+} concentrations. On the other hand limited rare-earth concentration should be used in order to avoid clusters formation with the consequent undesirable energy transfer processes that decrease the quantum efficiency of the $^4I_{3/2}$ excited state [15–19]. This compromise is in fact considered for phosphate glasses that have been investigated, showing a great potential for waveguide lasers and amplifier use [20, 21].

In this paper we describe the preparation and spectroscopic characterization of Er^{3+} containing phosphoniobate glasses in the $NaPO_3$–Nb_2O_5 system. Planar waveguides have been prepared by Na^+–Ag^+ ion exchange and the waveguide optical properties have been evaluated.

2. Experimental details

2.1. Glasses preparation

Glasses were prepared by melting/casting process. Table 1 shows chemical compositions of the $(100-x)NaPO_3$–xNb_2O_5 glasses, with $x = 11.1$, 14.3, 17.7, 21.2, 25.0, 29.0, and 33.3 mol%. Powder mixtures of p.a. $NaPO_3$, Nb_2O_5 were melted in Pt crucibles at 1100 °C for 30 min in an electric furnace in an air atmosphere. The molten mixtures were poured into pre-heated brass molds and annealed at 400 °C for 30 min. Er^{3+} doped samples were also prepared with composition (mol%) $(75-z)$ $NaPO_3$–$25Nb_2O_5$–zEr^{3+} with $z = 0.02$, 0.2, 0.5, 0.62, 1.2 mol%.

2.2. Waveguide fabrication

The sample's parallel surfaces were polished and ion exchange was performed for an Er^{3+} containing $75NaPO_3$–$25Nb_2O_5$ glass using $(100-y)KNO_3$–$yAgNO_3$ ($0.1 < y < 1$ mol%) molten salts. Optically polished glass slabs were immersed in the pre-heated molten salt at 345 °C during the appropriate period of time from 5 up to 120 min.

2.3. Characterization

Thermal analysis measurements were performed using a 1600 DTA cell. α-Al_2O_3 was used as reference sample. Open Pt–Au crucibles were used under an N_2 atmosphere. Fourier transform infrared spectroscopy (FT-IR) spectra from powdered samples were measured by the KBr pellet technique using a Perkin-Elmer Model 2000 FT-IR spectrometer. Raman spectra were collected in a Renishaw Raman Imaging Microscope System 3000 instrument.

^{31}P NMR spectra were obtained with a Varian INNOVATE 300 spectrometer by the CP-MAS technique; a reference of H_3PO_4 was used.

EPR measurements were carried out by using a Varian spectrometer E-line, operating at 9.13 GHz (X-band).

Refractive indices of the glasses samples and planar waveguides were measured for both transverse electric (TE) and magnetic (TM) polarizations with an m-line apparatus (Metricon Model 2010) on the basis of the prism coupling technique. A gadolinium garnet (GGG) prism with a refractive index of 1.9644 at 632.8 nm was used. The apparatus is equipped with Si and Ge detectors to collect the visible and NIR light, respectively. Two He–Ne lasers, operating at 543.5 and 632.8 nm, and one diode laser, operating at 1550 nm, were employed. The resolution in the determination of the angles synchronous with the propagation modes was 0.0075°.

The absorption spectra in the 400–2000 nm range were measured using a Varian Spectrometer (Cary Model 500) at room temperature.

Room temperature emission spectra were obtained under a continuous diode laser operating at 800 nm and with an argon ion laser operating at 488 nm as the excitation source, using a SPEX Fluorolog F2121 spectrofluorimeter and a Ge detector.

3. Results and discussion

3.1. Optical and structural properties

Some of the glass properties such as hygroscopic character, melting temperature and color were observed to depend on the Nb_2O_5 concentration. Phosphate glasses containing less than 11.1 mol% Nb_2O_5 are hygroscopic and they are not considered here.

Figure 1 shows some pictures of representative samples. Depending on the Nb_2O_5 content, different colors are obtained. For lower Nb_2O_5, purple samples are obtained. For higher contents, yellowish samples are obtained. Moreover the color of the higher Nb_2O_5 content sample also depends on the melting temperature. The initially yellowish samples become purple if the melting temperature is raised to 1400 °C. Color changes are reversible in the sense that if the purple sample obtained at 1400 °C is re-melted at 1100 °C, a yellowish sample is obtained.

Figure 2(a) shows the absorption spectra in the UV–visible range for samples melted at the same temperature (1100 °C). A broad absorption band centered at ∼536 nm is observed for samples N11, N14 and N17. The band intensity is reduced with increasing Nb_2O_5 concentration, being no longer observed for samples with Nb_2O_5 content higher than 21 mol%.

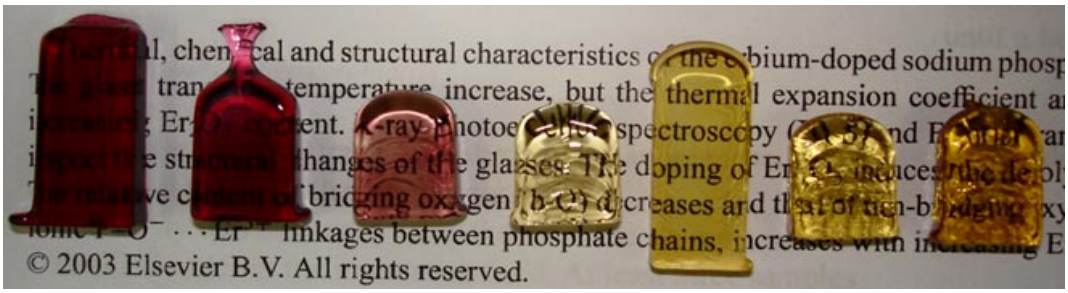

Figure 1. Images of typical glass samples: (a) N11, (b) N14, (c) N17, (d) N21, (e) N25, (f) N29, and (g) N33.

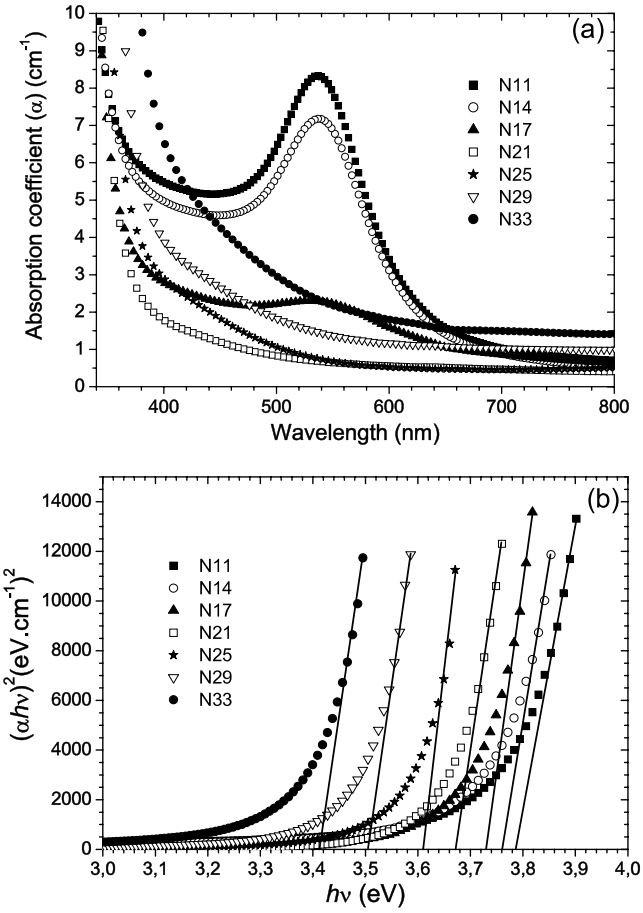

Figure 2. (a) Absorption spectra. (b) Absorption coefficient as a function of incident photon energy in the near band gap region. Samples are identified in the figure.

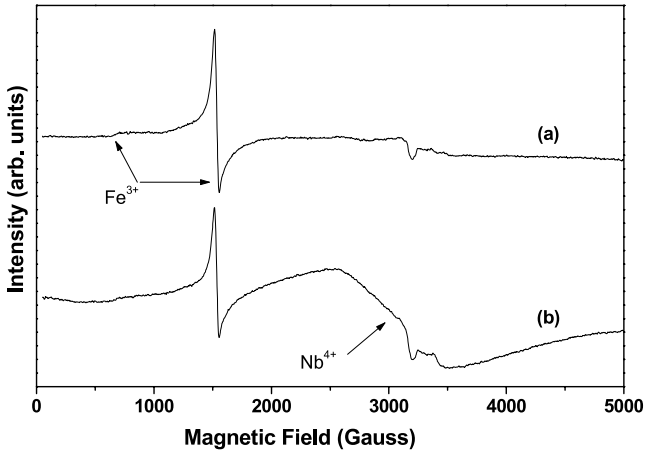

Figure 3. EPR spectra of the N33 glass sample prepared at: (a) 1100 °C, and (b) 1400 °C.

The different colors observed are related to the Nb atom oxidation state. d–d transitions cannot be observed in Nb^{5+} (d^0 configuration) materials. Therefore transparent materials are expected. However, the Nb^{4+} (d^1 configuration) can be observed in multicomponent borate, phosphate, germanate and silicate glasses (d^1) [22]. Non-stoichiometric oxides with general formula $Nb_2O_{5-\delta}$ can in fact be prepared with interesting conductivity and magnetic properties well related to the Nb^{4+} ion [23]. The color variation observed in the samples studied here could be related to the presence of Nb^{4+} which is in fact evidenced by the electron paramagnetic resonance (EPR).

Figure 3 shows EPR spectra for the N33 sample melted at two different temperatures, 1100 and 1400 °C. The spectrum obtained for the sample melted at 1100 °C, figure 3(a), shows a strong signal at 1550 G, corresponding to $g = 4.25$ and attributed to Fe^{3+} (natural impurity). A small signal at 650 G is also due to Fe^{3+} ($g = 9.5$). Another signal at 3200 G, $g = 2$, is related to some paramagnetic impurity of the sample or holder. The spectrum of the sample melted at 1400 °C, figure 3(b), shows the same Fe^{3+} signal, and an additional intense and broad signal at high field (FWHM = 1 kG) centered around 3050 G ($g = 2.15$), that can be attributed to the Nb^{4+} [22]. Interesting enough the $Nb^{5+} \leftrightarrows Nb^{4+}$ equilibrium seems to depend not only on the Nb_2O_5 content but also on the melting temperature. In the literature, valence changing effects on Li_2O–Nb_2O_5–P_2O_5 glasses are observed either under the effect of high energy radiation or in the presence of a reducing agent [22]. This last case must be operative here since EPR measurements show paramagnetic impurities that could in fact be involved in the Nb^{5+} reduction process.

Other optical properties, such as the band gap and the cut-off, were obtained indirectly from absorption spectra. Considering the high absorption region, the transmittance T followed a simple correlation with the absorption

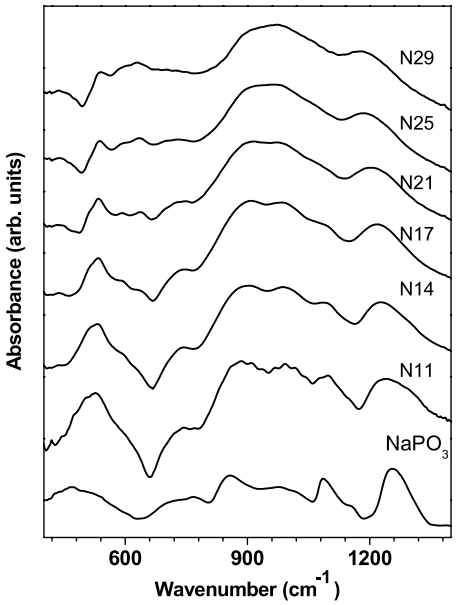

Figure 4. FT-IR spectra. Samples are identified in the figure.

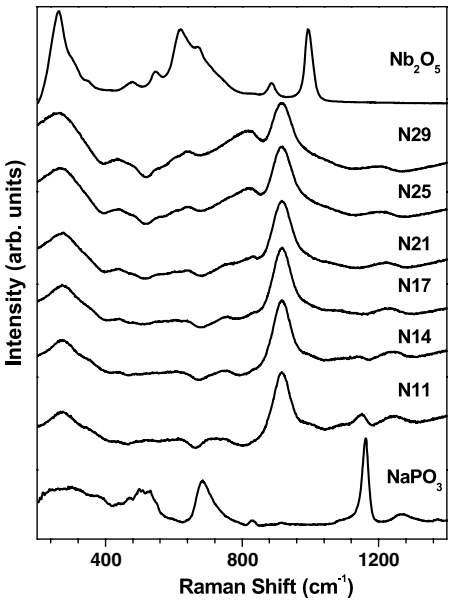

Figure 5. Raman spectra. Samples are identified in the figure.

coefficient [24, 25]:

$$T = A\exp(-\alpha d) \tag{1}$$

where A is approximately equal to the unity at the absorption edge and d is the thickness of the glass sample. The relation between the absorption coefficient α and incident photon energy $h\nu$ for allowed direct and indirect transitions, respectively, can be written as

$$\alpha h\nu = A_1(h\nu - E_g^1)^{1/2} \tag{2}$$

and

$$\alpha h\nu = A_2(h\nu - E_g^2)^2 \tag{3}$$

where A_1 and A_2 are two constants and E_g^1 and E_g^2 are the direct and indirect band gaps, respectively [24].

The $(\alpha h\nu)^2$ versus $h\nu$ plots for glasses containing different amounts of niobium are shown in figure 2(b). A linear behavior can be observed in a certain range of the curves, supporting the interpretation of a direct E_g^1 band gap for thin films [24, 25]. Therefore, the E_g^1 band gap of the glasses can be obtained by extrapolating relation (2) between 3.4 and 3.8 eV. Table 1 also shows the E_g^1 band gap values. The band gap decreases, from 3.79 to 3.41 eV, as the Nb_2O_5 content increases from 11.1 to 33.3 mol%. Similar results can be observed in the literature for $[xPb_3O_4–(1-x)P_2O_5]$ glasses with x varying from 0.075 to 0.4 [26].

Glass transition temperature (T_g) values were obtained from DTA curves not shown here. Table 1 shows a dramatic increase in the T_g values, ranging from 470 °C (N11) up to 710 °C (N33) with increasing Nb_2O_5 content. The Nb_2O_5 incorporation into the polyphosphate glass leads to structural changes that could be further investigated by spectroscopic methods.

Figures 4 and 5 show FT-IR and Raman spectra, respectively. Spectra obtained for $NaPO_3$ and Nb_2O_5 are shown as well. Table 2 summarizes the results. The data can be interpreted on the basis of previous publications on sodium polyphosphate [27], $NaPO_3$–WO_3 [28] and $NaPO_3$–MoO_3 [29] glasses. For pure $NaPO_3$ the FT-IR spectrum displays bands at 1256 cm^{-1} assigned to the asymmetric stretching, and at 1152 cm^{-1} (shoulder) assigned to symmetric stretching of the PO_2–metaphosphate (Q^2) units. The bands observed at 850 and 770 cm^{-1} are assigned to asymmetric and symmetric stretching modes of P–O–P linkages respectively. The broad band observed at 490 cm^{-1} is assigned to the O–P–O bending vibration. With increasing Nb_2O_5 content the 1255 cm^{-1} band shifts gradually, being observed at ∼1190 cm^{-1} for the N29 sample. The increasing contributions of new broad bands appearing at around 615 and 970 cm^{-1} hinder the observation of the polyphosphate bands. As suggested from T_g values, the polyphosphate chains are broken by the addition of Nb_2O_5 leading to the formation of P–O–Nb linkages.

As regards Raman results, the spectrum obtained for vitreous $NaPO_3$ displays two main bands at 1160 and 685 cm^{-1} that can be assigned to the (PO_2–) symmetric stretching vibration associated with the terminal oxygen

Table 2. Wavenumbers and tentative assignments for major FT-IR and Raman bands.

Wavenumber (cm^{-1})		
FT-IR	Raman	Vibrational mode
480–530	—	PO_4^{-3}
517	282	δ(O–P–O) + δ(O–Nb–O)
725–775	720	$(P–O–P)_s$
905	914	Nb–O
880–910	—	$(P–O–P)_{as}$
995–990	—	PO_4^{3-}
1080–1110	—	$P–O^-$
1160	1160	$(PO_2)_s$
1320–1350	—	P=O
1260–1280	—	$(PO_2)_{as}$

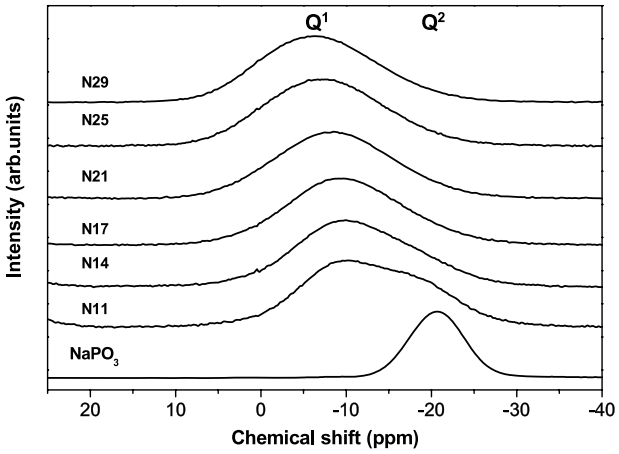

Figure 6. ^{31}P NMR spectra. Samples are identified in the figure.

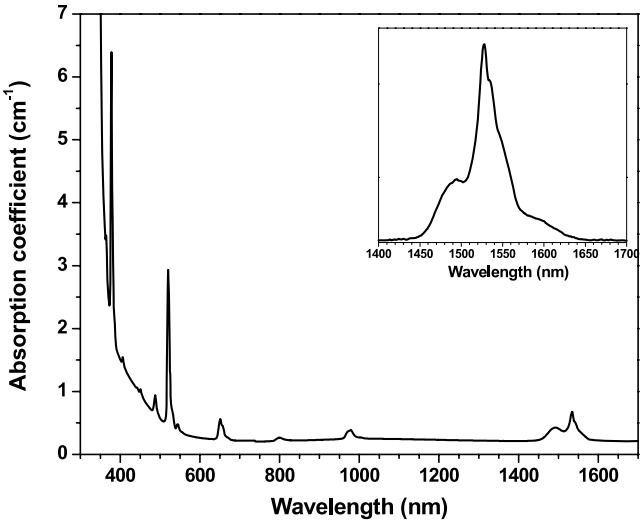

Figure 7. Room temperature absorption spectrum of the Er^{3+} doped (1.2 mol%) N25 sample. Inset—room temperature emission spectrum excited at 488 nm.

species and the symmetric P–O–P bond stretching vibration, respectively [28, 29]. With the Nb_2O_5 addition a new band at 916 cm^{-1} is observed. With increasing Nb_2O_5 content the 1160 cm^{-1} band shifts to lower wavenumbers and the 680 cm^{-1} one shifts to higher wavenumbers, both almost disappearing for the sample N17. For higher Nb_2O_5 content a new band appears at 825 cm^{-1}, increasing in intensity. In the low wavenumber region, weak bands at 637 and 433 cm^{-1} and a strong band at 265 cm^{-1} increase in intensity with the increase in the Nb_2O_5 content.

The bands at 916 and 825 cm^{-1} could be associated with terminal oxygen atoms associated with six-coordinate Nb atoms which is similar to the case for $NaPO_3$–WO_3 and $NaPO_3$–MoO_3 glasses studied before [28, 29]. The 825 cm^{-1} band gaining dramatically in intensity for higher Nb_2O_5 contents could be assigned to Nb–O stretching vibrations within Nb–O–Nb bond units.

Figure 6 shows ^{31}P NMR spectra obtained for the glasses and also the vitreous $NaPO_3$. A broad peak at −20.7 ppm is observed for the vitreous $NaPO_3$. With the addition of Nb_2O_5 this band is shifted to lower chemical shift and a new component appears at −10.3. A progressive shift and decrease in intensity for the higher chemical shift band is observed. For the highest Nb_2O_5 content (sample N29) a broad band is observed at −6.4 ppm. Good agreement is observed with results presented for similar glass compositions in [30]. Chemical shifts could be assigned, considering the usual Q^n notation where n stands for the number of bridging oxygens bonded to a given $[PO_4]$ site. In this way orthophosphate Q^0, pyrophosphate Q^1, metaphosphate Q^2, and ultraphosphate Q^3 units are related to bands appearing at around 14 ppm, between −6 and 6 ppm, between −32 and −16 ppm and between −36 and −54 ppm respectively. The positive chemical shift observed with increasing Nb_2O_5 content is related to the breakdown of the polyphosphate chains, as already suggested from FT-IR and Raman spectra.

The structural picture that can be extracted from these spectroscopic measurements is that starting from the metaphosphate structure (Q^2) of the $NaPO_3$ glass, the addition of Nb_2O_5 leads to a breakdown of the polyphosphate chains. Q^1 and Q^2 species are present in the samples with low Nb_2O_5 concentration. Only Q^1 species are present at higher Nb_2O_5 concentrations where Nb–O–Nb structures could be identified as well.

Figure 7 shows the absorption spectrum obtained for the N25 sample containing 1.2 mol% of Er^{3+} ions. The sharp absorption bands can be easily assigned to intraconfigurational 4f–4f transitions of the Er^{3+} ions, from the ground state $^4I_{15/2}$ to the excited states: $^4I_{13/2}$ (1532 nm, shoulder at 1545 nm), $^4I_{11/2}$ (973 nm), $^4I_{9/2}$ (796 nm), $^4F_{9/2}$ (650 nm), $^4S_{3/2}$ and $^4H_{11/2}$ (547 and 520 nm), $^4F_{7/2}$ (488 nm), $^4F_{5/2}$ (451 nm), $^2H_{9/2}$ (407 nm), $^2G_{11/2}$ (377 nm) and $^2G_{9/2}$ (365 nm) [10].

Relatively intense NIR emission was observed at room temperature and the emission spectrum is shown in the inset of figure 7. The spectrum was collected under 488 nm excitation from an argon ion laser, exciting directly the $^4F_{7/2}$ excited state of the Er^{3+} ions. The emission band, with a maximum at 1528 nm and shoulders at 1492 and 1598 nm, with 32.7 nm bandwidth, corresponds to the $^4I_{13/2} \rightarrow {}^4I_{15/2}$ transition and is comparable with those for other phosphate systems shown in the literature. No change was observed using as excitation source a diode laser operating at 800 nm. The production of glasses with low OH content is responsible for the high luminescence signal at 1528 nm, where the contribution to the non-radiative process through multiphonon relaxation process is reduced. The introduction of niobium oxide to polyphosphate glasses gives rise to chemically stable OH-free phosphate systems.

Lifetime values were obtained by fitting single-exponential functions to the decay curves obtained for the emission at 1528 nm and figure 8 shows the evolution of the lifetime values, obtained from the fits, as a function of the Er^{3+} concentration. A value of 5.4 ± 0.5 ms is obtained for the lowest Er^{3+} concentration and is observed for concentrations up to 0.2 mol%. For higher concentrations, lifetime values decrease and reach a value of 2.4 ± 0.3 ms for the sample of highest

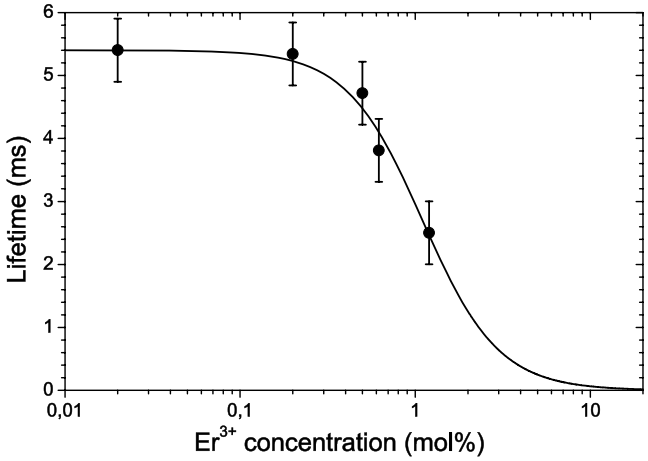

Figure 8. Emission lifetime values (ms) as a function of the Er^{3+} content. Emission at 1530 nm and excitation at 488 nm. Experimental points are fitted with equation (4) with $\tau_0 = 5.402$ ms; $Q = 1.1$ mol% Er^{3+} and $p = 2$.

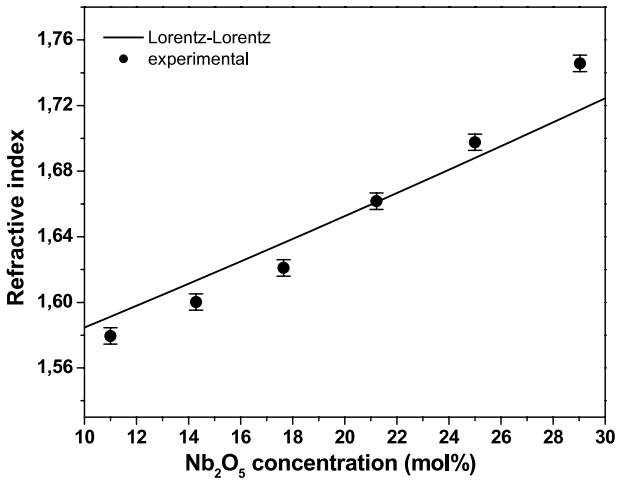

Figure 9. Refractive index measured at 632.8 nm as a function of the Nb_2O_5 content. The solid line is a theoretical fit using the Lorentz–Lorentz equation.

concentration (1.2 mol%) following the trends observed in other glass systems [15, 16, 31–33].

The experimental values could be fitted to empirical formulas [31]:

$$\tau_{\text{exp}} = \frac{\tau_0}{1 + \left(\frac{C_{Er^{3+}}}{Q}\right)^P}, \tag{4}$$

where τ_{exp} is the experimental lifetime, τ_0 is the lifetime for zero-concentration limit, $C_{Er^{3+}}$ is the Er^{3+} concentration, Q is the so called 'quenching concentration' for which the lifetime is reduced by 50% from the zero-concentration limit, and P is a phenomenological parameter characterizing the steepness of the quenching curve, expected to be ∼2 for a two-ion cross-relaxation mechanism. From the fit, shown in figure 8, the following values could be obtained: $\tau_0 = 5.402$ ms, $Q = 1.1$ mol% (1.45×10^{20} ions cm^{-3}), and $P = 2$.

The quenching concentration is higher than the one found before for the Er^{3+}/Yb^{3+} codoped phosphoniobate glass matrix ($Q = 0.6$ mol%) [10] and other silicate systems like the SiO_2–HfO_2 ($Q = 0.81$ mol%) [32], the SiO_2–TiO_2–Al_2O_3 [31].

The value obtained for the radiative lifetime (5.4 ms) is close to the values observed for the less concentrated samples (up to 0.2 mol%), suggesting that in those samples, interaction between Er^{3+} ions and multiphonon decay is negligible and the emission quantum efficiency is about 90%. With increased Er^{3+} concentration, the emission quantum efficiency decreases to the value of 35% obtained for the 1 mol% Er^{3+} sample, mainly due to ion–ion interactions, such as energy migration and cooperative up-conversion [15, 16].

3.2. Waveguiding properties of the ion exchanged glasses

Figure 9 shows the refractive index values of the glasses, measured at 632.8 nm as a function of the Nb_2O_5 content. An increase from 1.560 (sample N11) to 1.746 (sample N29) is observed. The refractive index measured in TE and TM polarization does not change, indicating a negligible birefringence in this vitreous system. Moreover the refractive index values which are close to the values calculated by using the Lorentz–Lorentz equation [34], by considering the refractive index values for niobium oxide (2.3) and sodium phosphate (1.50), as also shown in figure 9. These results indicate a fully densified material without residual porosity or water absorbed.

The N25 composition has been chosen for planar waveguide fabrication. Exchanging times ranging from 5 to 120 min were used together with Ag^+ content varying from 0.1 to 1.0 mol% in the exchanging bath. In general short times were observed to be enough to produce a waveguide with ideal diffusion depth to well confine one mode at 1550 nm. Some results for the optical parameters obtained for different exchanging time and Ag^+ concentration are summarized in table 3. For 10 min of exchanging time the diffusion profile was observed to be over 10 μm and the number of guided modes over 2.

For 0.1 mol% Ag^+ and 5 min of ionic exchange a monomode condition was observed at 1550 nm (sample N25–C1). Figure 10 shows the refractive index profile of that waveguide reconstructed from the effective indices at 632.8 nm by an inverse Wentzel–Kramers–Brillouin method [35]. A graded index profile was observed and the difference between the refractive index profiles obtained for TE and TM polarization modes indicates a low birefringence in this waveguide.

Energy dispersive x-ray analysis (EDX) were performed for the same sample and figure 11 shows the results as Ag^+/Na^+ and K^+/Na^+ peaks area ratios. The relative Ag^+ concentration is reduced from the substrate surface to the bulk, resulting in a graded concentration profile. However the refractive index profile is observed to be related not only on the Ag^+ concentration profile but also on the K^+ concentration profile. Studies of the absolute values of K^+ and Ag^+ ion concentrations are in progress, in order to better correlate the refractive index profile and diffusion process.

Table 3. Optical parameters of the investigated planar waveguides as a function of the ion exchange conditions. Sample—Er^{3+} doped (1.2 mol%) N25. Conditions: N25–C10: $[Ag^+] = 0.1$ mol%, $t = 5$ min; N25–C2: $[Ag^+] = 0.1$ mol%, $t = 10$ min; N25–C3: $[Ag^+] = 0.5$ mol%, $t = 5$ min; N25–C4: $[Ag^+] = 1.0$ mol%, $t = 10$ min. Refractive index η (± 0.0005) of the base glass—1.6740 (543.5 nm); 1.6661 (632.8 nm); 1.6394 (1550 nm).

Sample			N25–C1	N25–C2	N25–C3	N25–C4
$\lambda = 543.5$ nm	η	TE	1.6806	1.6805	1.7476	1.8060
		TM	1.6830	1.6829	1.7497	1.8075
	Number of modes		4	5	>6	>6
$\lambda = 632.8$ nm	η	TE	1.6721	1.6719	1.7371	1.8005
		TM	1.6738	1.6729	1.7389	1.8011
	Number of modes		3	4	>5	>5
$\lambda = 1550$ nm	η	TE	1.6428	1.6444	1.6962	1.7499
		TM	1.6438	1.6458	1.6983	1.7515
	Number of modes		1	2	>5	>5
Thickness (± 0.1 μm)			5.9	9.9	~16	>16

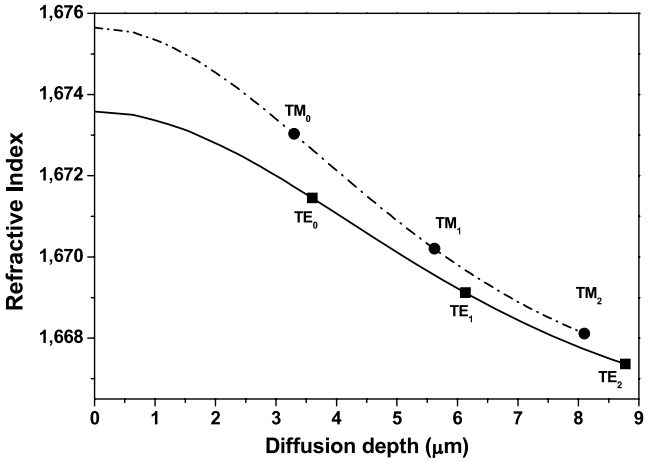

Figure 10. Refractive index profiles of the N25–C1 planar waveguide reconstructed from modal measurements at 633 nm for TE and TM polarizations. The effective indices of the $TE_{0,1,\text{ and }2}$ (closed squares) and $TM_{0,1,\text{ and }2}$ (closed circles) modes are illustrated.

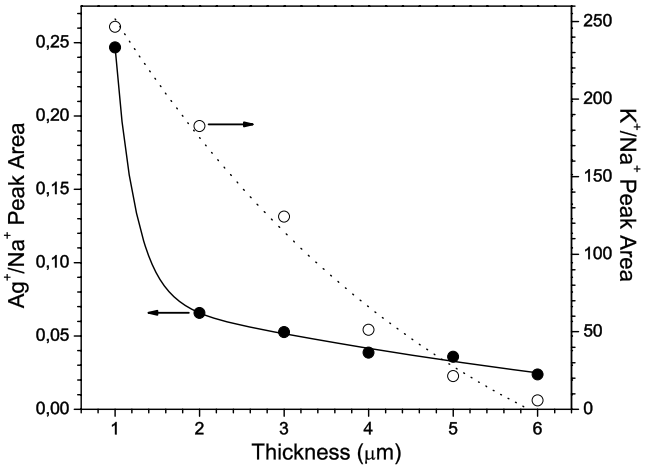

Figure 11. EDX results represented as the ratio between Ag^+/Na^+ and K^+/Na^+ peak areas after ion exchange of the N25–C1 material. The line is a guide for the eye.

Figure 12(a) shows the calculated near field intensity distribution in the monomodal waveguide (TE mode) for 1550 nm, with a width of 10 μm, and the refractive index and thickness of the N25–C1 sample. This simulation was carried out using the software developed by Hammer [36]. A high confinement coefficient of the TE_0 mode is expected, meaning that an efficient injection at 1550 nm is possible for the waveguide produced. Figure 12(b) shows the squared electric field profiles of the TE_0 and TM_0 modes of the same waveguide, calculated at 1550 nm by using the parameters obtained from the m-line measurements. The modeling indicates that the optical parameters of the waveguide, i.e., refractive index and thickness, appear appropriate for application in the third telecommunication window, with confinement coefficients of 72% and 78% for TE_0 and TM_0 modes, respectively.

4. Conclusions

In summary, the preparation of stable and non-hygroscopic glasses in the $NaPO_3$–Nb_2O_5 system was described. Different glass colors were observed, depending on melting temperature and glass composition. The presence of Nb^{4+} detected via EPR measurements accounts for the colors observed.

The addition of Nb_2O_5 to sodium polyphosphate glass leads to important structural changes, producing more stable glasses, and increasing the glass transition temperature. The respective increase in the refractive index values could be well simulated by considering the Lorentz–Lorentz expression.

FT-IR, Raman and ^{31}P NMR results clearly show that the Nb_2O_5 incorporation leads to a breakdown of the fully Q^2 polyphosphate network. Q^1 units together with Nb–O–Nb interaction could be identified for the Nb_2O_5 rich glasses.

Er^{3+} containing samples were prepared and relatively intense NIR emission was observed in the 1550 nm region. The emission quantum efficiency was observed to be around 90% for the lower Er^{3+} concentrations. The concentration quenching was observed to be $Q = 1.1$ mol% (1.45×10^{20} ions cm^{-3}).

Planar waveguides were obtained by ion exchange at 345 °C in a KNO_3–$AgNO_3$ melt. The synthesized waveguides could support single modes and multimodes depending on thickness, refractive index, and excitation wavelength. The

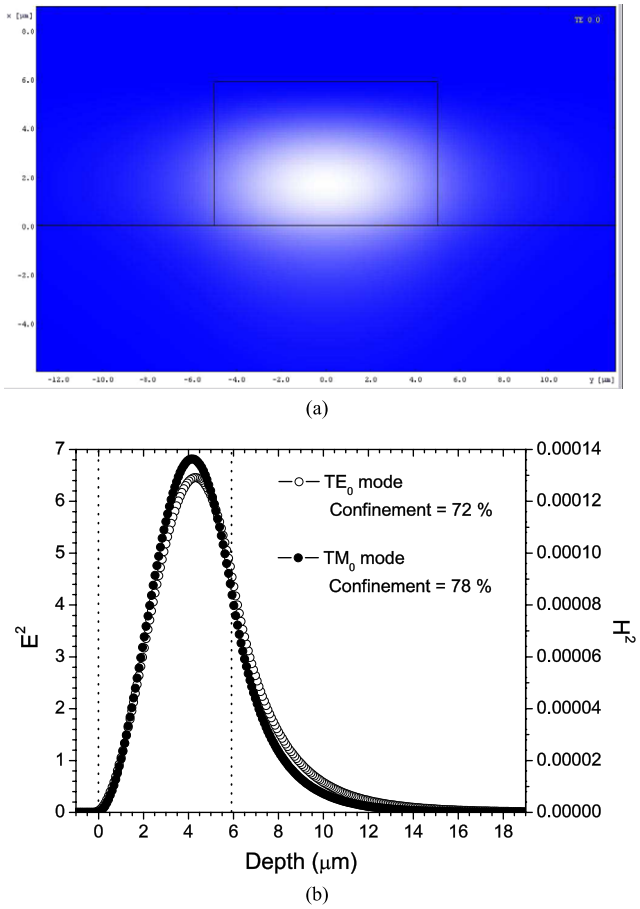

Figure 12. (a) Simulated near field intensity distribution of TE_0 mode at 1550 nm for a monomodal channel waveguide of the N25–C1 sample with 10 μm width (2D profile); (b) calculated squared electric field profiles of the TE_0 and TM_0 modes at 1550 nm.

experimental parameters of the ion exchange technique such as Ag^+ ion concentration and exchange time control the refractive index and thickness of the resulting waveguide. This procedure was optimized in order to obtain single-mode waveguides at 1550 nm. An exchange time of just 5 min at 345 °C, in a bath with composition (mol%) $99.9KNO_3$–$0.01AgNO_3$, was used. Ag^+ ions together with K^+ ions were observed to contribute to the graded index profiles obtained.

Acknowledgments

The Brazilian agencies CNPq, CAPES, and FAPESP are acknowledged for financial support.

References

[1] Desurvire E 1994 *Erbium-Doped Fiber Amplifiers* (New York: Wiley)
[2] Mears P J, Reekie L, Jauncey I M and Payne D N 1987 *Electron. Lett.* **23** 1026
[3] Jose G, Sorbello G, Taccheo S, Cianci E, Foglieti V and Laporta P 2003 *J. Non-Cryst. Solids* **322** 256
[4] Kik P G and Polman A 1998 *MRS Bull.* **23** 48
[5] Brown R K 2000 *J. Non-Cryst. Solids* **263** 1
[6] Khafagy A H, El'Rabaie S M, Higazy A A and Eid A S 2000 *Indian J. Phys.* A **74** 433
[7] Sales B C and Boatner L A 1987 *J. Am. Ceram. Soc.* **70** 615
[8] Key W S and Miller J C 1994 Phosphate glass for photonics *ORNL Rev.* **27** 12
[9] Yan Y C, Faber A J, de Waal H, Kik P G and Polman A 1997 *Appl. Phys. Lett.* **71** 2922
[10] Barbosa A J, Dias Filho F A, Messaddeq Y, Ribeiro S J L, Gonçalves R R, Luthi S R and Gomes A S L 2006 *J. Non-Cryst. Solids* **352** 3636
[11] Righini G C, Pelli S, Ferrari M, Armellini C, Zampedri L, Tosello C, Ronchin S, Rolli R, Moser E, Montagna M, Chiasera A and Ribeiro S J L 2002 *Opt. Quantum Electron.* **34** 1151
[12] Jose G, Sorbello G, Taccheo S, Della Valle G, Cianci E, Foglietti V and Laporta P 2003 *Opt. Mater.* **23** 559
[13] Ramponi R, Osellame R, Marangoni M, Sorbello G, Laporta P, Jiang S, Hu Y and Peyghambarian N 2000 *Opt. Mater.* **14** 291
[14] Ramaswamy R V 1988 *J. Lightwave Technol.* **6** 984
[15] Delavaux J M P, Granlund S, Mizuhara O, Tzeng L D, Barbier D, Rattay M, Saint-André F and Kevorkian A 1997 *IEEE Photon. Technol. Lett.* **9** 24729
[16] van den Hoven G N, Snoeks E, Polman A, van Dam C, van Uffelen J W M and Smit M K 1996 *J. Appl. Phys.* **79** 1258
[17] Myslinski P, Nguyen D and Chrostowski J 1997 *J. Lightwave Technol.* **15** 112
[18] Auzel F and Goldner P 2001 *Opt. Mater.* **16** 93
[19] Vallés J A, Lázaro J A and Rebolledo M A 2002 *IEEE J. Quantum Electron.* **38** 318
[20] Kik P G and Polman A 1998 *MRS Bull.* **23** 48
[21] Veasey D L, Funk D S, Peters P M, Sanford N A, Obarski G E, Fontaine N, Young M, Peskin A P, Liu W C, Houde-Walter S N and Hayden J S 2000 *J. Non-Cryst. Solids* **263** 369
[22] Aleksandrow A I, Bubnov N N and Prokof A I 1995 *Appl. Magn. Reson.* **9** 251
[23] Cava R J, Batlogg B, Krajewski J J, Poulsen H F, Gammel P, Peck W F Jr and Rupp L W Jr 1991 *Phys. Rev.* B **44** 6973
[24] Pal U, Samanta D, Ghorai S and Chaudhuri A K 1993 *J. Appl. Phys.* **74** 6368
[25] Maia L J Q, Bernardi M I B, Feitosa C A C, Mastelaro V R, Zanatta A R and Hernandes A C 2004 *Thin Solid Films* **457** 246
[26] Salagram M, Prasad V K and Subrahmanyam K 2002 *Opt. Mater.* **18** 367
[27] Hudgens J J, Brow R K, Tallant D R and Martin S W 1998 *J. Non-Cryst. Solids* **223** 21
[28] Santagneli S H, Araujo C C, Strojek W, Eckert H, Poirier G, Ribeiro S J L and Messaddeq Y 2007 *J. Phys. Chem.* B **111** 10109
[29] Araujo C C, Strojek W, Zhang L, Eckert H, Poirier G, Ribeiro S J L and Messaddeq Y 2006 *J. Mater. Chem.* **16** 3277
[30] Flambard A, Montagne L, Delevoye L, Palavit G, Amoreux J P and Videau J J 2004 *J. Non-Cryst. Solids* **345** 75
[31] Orignac X, Barbier D, Du X M, Almeida R M, McCarthy O and Yeatman E 1999 *Opt. Mater.* **12** 1
[32] Francini R, Giovenale F, Grassano U M, Laporta P and Taccheo S 2000 *Opt. Mater.* **13** 417
[33] Gonçalves R R, Carturan G, Montagna M, Ferrari M, Zampedri L, Pelli S, Righini G C, Ribeiro S J L and Messaddeq Y 2004 *Opt. Mater.* **25** 131
[34] Lorentz H A 1909 *Theory of Electrons* (Leipzig: Teubner)
[35] Chiang K S 1985 *J. Lightwave Technol.* **3** 385
[36] Hammer M, 2D multilayer waveguide mode solver effective index approximation http://wwwhome.math.utwente.nl/~hammer/eims.html